Applied Catalysis B: Environmental 266 (2020) 118669

Contents lists available at ScienceDirect

Applied Catalysis B: Environmental

journal homepage: www.elsevier.com/locate/apcatb

Essential role of oxygen vacancies of Cu-Al and Co-Al spinel oxides in their catalytic activity for the reverse water gas shift reaction

Ali M. Bahmanpour[a], Florent Héroguel[a], Murat Kılıç[a], Christophe J. Baranowski[a], Pascal Schouwink[a], Ursula Röthlisberger[a], Jeremy S. Luterbacher[a], Oliver Kröcher[a,b,*]

[a] Institute of Chemical Sciences and Engineering, École Polytechnique Fédérale de Lausanne (EPFL) 1015 Lausanne, Switzerland
[b] Paul Scherrer Institut (PSI), 5232 Villigen, Switzerland

ARTICLE INFO

Keywords:
CO_2hydrogenation
Copper
Spinel
Oxygen vacancy
Cobalt

ABSTRACT

CO_2 catalytic hydrogenation to CO will likely be an important part of CO_2 mitigation and valorization processes. Recently, we have developed materials containing surface-formed Cu-Al spinel that act as active and stable catalysts for this reaction. Here, the fundamental characteristics of Cu-Al and Co-Al spinel catalysts were studied to understand the role of the spinel structure in its catalytic activity for the reverse water gas shift reaction. Based on the catalytic tests, Cu-Al spinel was found to have a higher catalytic activity. By means of catalysts characterization combined with theoretical studies, this increased activity was attributed to the higher number of oxygen vacancies on its surface which were formed because of the higher inversion degree of Cu-Al spinel, which in turn, resulted in the formation of a more disordered structure with cation substitution. We found that the oxygen vacancies were vital for CO_2 adsorption and activation on the spinel surfaces.

1. Introduction

Catalytic conversion of CO_2 to value-added chemicals has been frequently investigated because CO_2 excess emissions have caused catastrophic environmental effects including climate change, and ocean acidification [1]. Although important steps have been taken in CO_2 direct conversion to methanol as a green fuel, this process still results in low methanol yield due to the high stability of CO_2 [2,3]. Alternatively, conversion of CO_2 to CO, which in thermal catalysis proceeds through the reverse water gas shift (RWGS) reaction, has gained increasing attention because it is a promising route for CO_2 recycling and valorization through synthesis gas production using renewable hydrogen. Unlike CO_2 which is thermodynamically stable, CO is much more active and its further conversion to various chemicals is well known [4,5]. Through this reaction, the CO/CO_2 ratio of the resulting synthesis gas can be tuned. Besides the advantages of the RWGS reaction, studying this reaction is of high interest, particularly, since it is known that CO is formed as an intermediate product in CO_2 hydrogenation reactions that aim to form other chemicals such as methanol [6,7]. Cu-based and other transition and noble metallic catalysts are among the most attractive ones for this reaction due their relatively high activity and high selectivity towards CO [3,8,9]. However, Cu-based catalysts lack stability at the relatively high temperatures (> 400 °C) required for this reaction [8,10,11]. Much progress has been made to improve the metal-based catalysts for the RWGS reaction. Notably, the addition of promoters such as K or Fe to the supported Pt-based and Cu-based catalysts was shown to improve their activity through formation of new active sites at the interface of the metal and the promoter [11–13]. Many catalytic supports such as alumina, silica, saponite clay, titania, ceria, or more uncommon materials such as molybdenum carbide have been proposed to increase Ni and Cu dispersity in order to improve their activity in both the RWGS [10,14–19] and the WGS [20,21].

Recently, our research group has presented a surface-formed Cu-Al spinel catalyst as a promising candidate for CO_2 conversion to CO [22]. Unlike other copper-based catalysts, this catalyst has shown both high activity and high stability while running the RWGS reaction. Therefore, comparing the activity of Cu-Al spinel to other spinel catalysts formed with other active transition metals in the RWGS reaction would be particularly interesting. Cobalt is a known active catalyst for CO_2 hydrogenation [23,24] and the RWGS reaction [25] and CO_2 was previously reported to be activated on the surface of the Co-Al spinel catalyst [26]. Therefore, we have investigated and compared the catalytic activity of Cu-Al and Co-Al spinel catalysts. Through this study, we investigated the fundamental reasons behind the observed

* Corresponding author at: Institute of Chemical Sciences and Engineering, École Polytechnique Fédérale de Lausanne (EPFL) 1015, Lausanne, Switzerland. Paul Scherrer Institut (PSI), 5232 Villigen, Switzerland.
E-mail address: oliver.kroecher@psi.ch (O. Kröcher).

https://doi.org/10.1016/j.apcatb.2020.118669
Received 6 November 2019; Received in revised form 17 January 2020; Accepted 21 January 2020
Available online 27 January 2020

differences in their activity. We found that Cu-Al spinel outperformed Co-Al due to the higher concentration of surface oxygen vacancies that were formed on its surface because of the higher degree of inversion of Cu-Al spinel. This result highlights the prominent role of oxygen vacancies in CO_2 activation on spinel catalysts.

2. Experimental

2.1. Catalysts synthesis

Both Cu-Al and Co-Al spinel catalysts were synthesized using the co-precipitation method followed by calcination [27]. $Cu(NO_3)_2{\cdot}3H_2O$ (ABCR) and $Al(NO_3)_3{\cdot}9H_2O$ (Sigma-Aldrich) were used as the copper and aluminum precursors. The two salts were dissolved using a 2:1 M ratio of Al:Cu in milli-Q water and mixed together. A 1 M aqueous solution of Na_2CO_3 was used as the precipitating agent, which was added to the salt mixture dropwise at room temperature. The formed suspension was then stirred at 75 °C for 6 h and filtered and washed thoroughly. The resulting sample was dried overnight at 120 °C. The dried powder was calcined at 900 °C for 5 h, which is the minimum temperature for spinel formation [28–30]. In the case of the Co-Al spinel synthesis, $Co(NO_3)_2{\cdot}6H_2O$ (Sigma-Aldrich) was used as the cobalt precursor. The rest of the procedure was the same. Alkaline treatment was used to create further oxygen vacancies in the Co-Al catalyst [31]. The alkaline treated Co-Al catalyst (Co-Al-AT) was prepared by treating 0.2 *g* of Co-Al with 30 mL of a 1 M aqueous NaOH solution at room temperature for 30 min. The resulting suspension was centrifuged and washed thoroughly and was then dried at 120 °C for 4 h before the reaction.

2.2. Catalytic activity tests

The catalytic tests were done using a gas-phase setup equipped with a fixed bed quartz reactor and an online MATRIX-MG01 FTIR spectrometer (Bruker) equipped with a 10 cm gas cell, which was heated at 120 °C. The obtained spectra were analysed using the OPUS-GA software. The desired amount of catalyst was placed in the reactor and fixed with quartz wool. For each run, the catalyst was dried *in situ* at 150 °C under Ar flow for 30 min before the reaction. A flow of H_2 (10 mL·min^{-1}) and CO_2 (5 mL·min^{-1}) diluted in Ar (50 mL·min^{-1}) was then introduced to the reactor, which was heated to the desired temperature using heating wires.

2.3. Catalyst characterization

Brunauer-Emmett-Teller (BET) surface and Barrett-Joyner-Halenda (BJH) mesoporous volumes were calculated from N_2-physisorption measurements on a Micromeritics 3Flex apparatus at liquid nitrogen temperature between 10^{-5} and 0.99 relative N_2 pressure. Samples (ca. 100 mg) were dried at 120 °C (temperature reached with a ramp of 2 °C·min^{-1}) under vacuum ($< 10^{-3}$ mbar) for 4 h and a leak test was performed prior to analysis.

Temperature-programmed reduction (H_2-TPR) was performed on a Micromeritics Autochem II 2920. Typically, 0.2 g of sample were treated with a 90:10 Ar:H_2 mixture and the sample temperature was ramped to 800 °C (10 °C·min^{-1}). H_2 consumption was measured using a calibrated Thermal Conductivity Detector (TCD).

CO_2-TPD was performed on the same setup, which was used for the catalytic test. 0.1 g of each catalyst were fixed in the quartz reactor and dried at 120 °C (temperature ramp of 10 °C·min^{-1}) for 30 min before the CO_2 exposure. The temperature was then cooled down to 30 °C under Ar flow and then the flow was switched to 50 mL·min^{-1} of pure CO_2 for 1 h. The flow was then switched back to Ar and the reactor was purged for 1 h to eliminate any physisorbed CO_2. The temperature was then increased to 800 °C with a ramp of 10 °C·min^{-1}. The concentrations of CO and CO_2 were monitored using the online FTIR spectrometer described earlier.

The temperature diffuse reflectance infrared Fourier transform (DRIFT) spectra were recorded using a high temperature Harrick DRIFT cell mounted on a Perkin Elmer Frontier spectrometer equipped with a mercury cadmium telluride detector. Samples were dried for 1 h under a 20 mL·min^{-1} He flow at 120 °C. After cooling down to 25 °C, the sample was exposed to CO_2 and purged with He. The temperature was ramped-up with a 5 °C·min^{-1} ramp rate while collecting spectra regularly. Spectra were recorded with 32 scans at a resolution of 4 cm^{-1}. The *in-situ* test was conducted by co-feeding of a CO_2 and H_2 mixture (100 mL·min^{-1}) at 250 °C and the temperature was increased to 350 °C.

X-ray photoelectron (XP) spectra were acquired using a PHI VersaProbe II scanning XPS microprobe (Physical Instruments AG, Germany). Measurements were done using a monochromatic X-ray source of 24.8 W power and a beam size of 100 µm. The spherical capacitor analyzer was set to the take-off angle of 45° relative to the sample surface. OriginPro 2017 software was applied for peak deconvolution.

X-ray diffraction data were collected in Bragg Brentano geometry on a D8 Bruker Discover diffractometer equipped with a non-monochromated Cu-source and a LynxEye XE detector. As these data were used for Rietveld refinement of the inversion degree, Debye-Scherrer measurements were performed additionally as a control to eliminate the possibility of preferred orientation by comparison between reflection and transmission data. Rietveld refinement was done with the Topas software [32]. The instrumental resolution was collected at the SRM1976b standard. The measured data were profile-fitted to obtain the empirical resolution function, which was then used to obtain domain sizes from integral breadths on the sample data. The background, height displacement, zero-error, spinel lattice parameters, 3 isotropic thermal displacement parameters (1 per Wyckoff site) and the inversion degree were described with a total of 8 parameters.

2.4. Computational methods

All Density Functional Theory (DFT) calculations were performed using the pw.x code of Quantum ESPRESSO (v.6.3) [33]. The Generalized Gradient Approximation (GGA) to DFT in the Perdew – Burke – Ernzerhof (PBE) formulation was used to optimize the lattice parameters and atomic configuration of all structures [34]. Ultra-soft pseudopotentials were used to describe the interaction between the core and the (semi) valence electrons for all of the atoms. The Kohn-Sham orbitals and total electronic density were extended in a plane wave basis with 130 and 630 Ry energy cutoffs, respectively.

For both systems, we sampled a (1 × 1 × 1) slab with 10 Å vacuum in order to separate the periodic images with a 4 × 4 × 1 Monkhorst - Pack *k*-point grid [35]. The (2 × 2 × 1) super cells with the same vacuum separation were modeled with a 2 × 2 × 2 *k*-point mesh. These values were selected by examining the convergence of the total energy ($\sim 10^{-3}$ Ry atom^{-1}) and atomic forces ($\sim 10^{-4}$ Ry au^{-1}). Both surface models (containing 224 atoms) were built based on a (100) surface. The optimized cell parameter was a box of 16.52 Å × 16.52 × 18.26 Å for $CuAl_2O_4$ and 16.12 Å × 16.12 × 18.06 Å for $CoAl_2O_4$.

3. Results and discussion

3.1. Catalytic activity

In order to maintain the spinel surface during the reaction, H_2-TPR was conducted to determine the temperature range, at which the catalytic test could be performed without reducing the spinel surface (Fig. 1a). No reduction peak for Co-Al spinel was observed up to 800 °C while Cu-Al spinel interacted with H_2 at ca. 400 °C. Although copper was not reduced to Cu° even at 800 °C (based on N_2O titration), we investigated the reaction at lower temperatures to ensure the Cu-Al spinel was not reduced. Therefore, the RWGS reaction was conducted

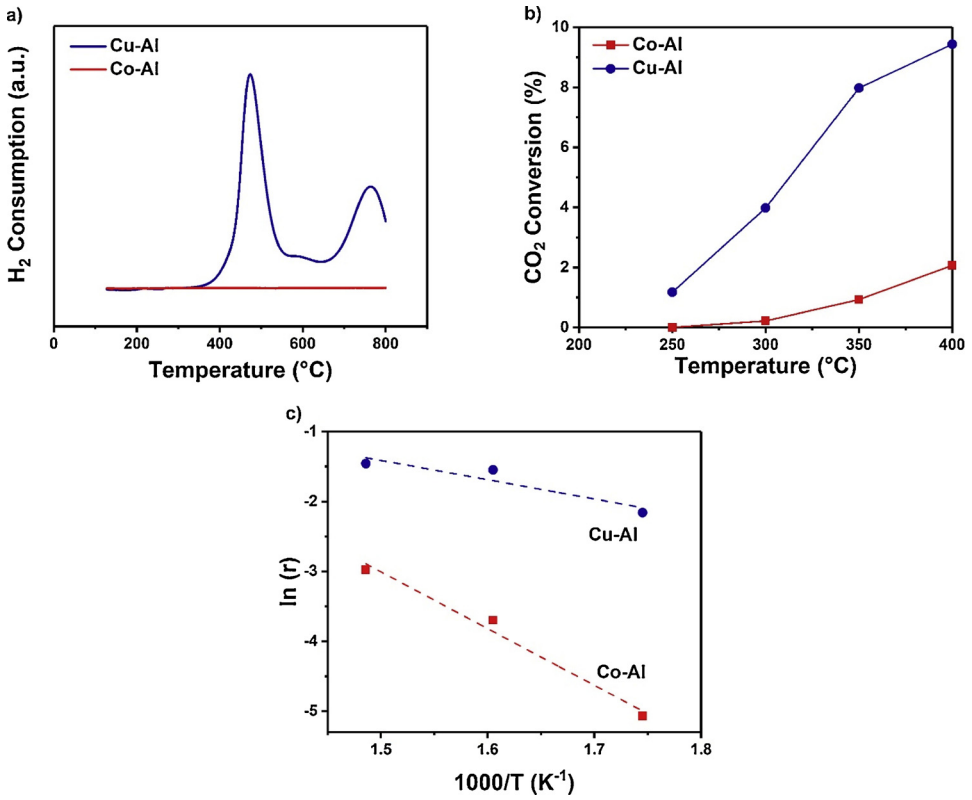

Fig. 1. a) H_2-TPR profile for Co-Al and Cu-Al spinel catalysts. b) Catalytic activity of the Co-Al and Cu-Al spinel catalysts. c) Arrhenius plot for the Co-Al and Cu-Al spinel catalysts.

on both catalysts between 250 °C–400 °C (Fig. 1b). In both cases, 100 % selectivity towards CO was achieved. Through the whole temperature range tested, the Cu-Al spinel showed higher activity despite its lower surface area and larger crystallite domain size (Table S1 and Figs. S1–S3 in the Supplementary Information). At 300 °C, CO_2 conversion using Cu-Al catalyst was about eight times higher compared to Co-Al. However, lower CO_2 conversion was achieved in the present study in comparison with our previous one [22]. This is due to the lower operating temperature, which affects both the reaction thermodynamics and the CO_2 desorption (discussed below), as well as the lower catalyst surface area. Rates of reaction were measured in the temperature range of 250–400 °C (Table S2), based on which an Arrhenius regression was calculated (Fig. 1c). A lower activation energy was calculated for the Cu-Al spinel compared to the Co-Al spinel (22.9 and 67.5 $kJ{\cdot}mol^{-1}$ for Cu-Al and Co-Al, respectively).

3.2. CO_2 adsorption/interaction

Since hydrogen did not measurably interact with the catalysts surfaces within the investigated temperature range, we concluded that the difference in activity between the two catalysts was due to a difference in CO_2 adsorption and activation, which could be a vital step in determining the catalyst activity for the RWGS reaction. To investigate this further, CO_2-TPD tests were conducted using both catalysts. First, we observed that no CO_2 desorbed from the surface of these two catalysts after purging of the physisorbed CO_2. With the Co-Al spinel, only CO desorbed at high temperatures (400–800 °C) (Fig. S4). CO desorption hinted that CO_2 adsorption might occur on oxygen vacancies of the Co-Al spinel where an oxygen atom fills the vacancy and remains on the surface after desorption of the CO. Neither CO_2 nor CO were desorbed from the Cu-Al spinel below 800 °C during the CO_2-TPD experiment. In order to confirm the presence of CO_2 on the catalyst surface, H_2 was introduced at 800 °C, which led to measurable CO desorption confirming that CO_2 was indeed adsorbed on the surface even at 800 °C.

Such strong CO_2 interactions for both catalysts is quite uncommon for surface adsorption. Therefore, CO_2 was likely filling a vacancy in the catalyst structure rather than a simple surface chemisorption. In both cases, physisorbed CO_2 might have desorbed during the purging step before starting the temperature ramp. The literature also suggests that CO_2 adsorbs on oxygen vacancies when using spinels as catalysts [36]. To verify CO_2 adsorption on the catalyst surface, DRIFT spectra were acquired during CO_2 adsorption. After drying at 150 °C, CO_2 was introduced at 30 °C and purged by Ar to remove the physisorbed and gaseous CO_2 (Fig. 2a). Increasing the temperature up to 400 °C did not result in desorption of the adsorbed CO_2, which agreed with the CO_2-TPD results. Two distinct peaks at 1270 cm^{-1} and 1606 cm^{-1} were observed upon CO_2 adsorption, which were assigned to bidentate carbonate [37]. The bidentate carbonate was likely formed due to the adsorption of CO_2 directly into the oxygen vacancy of the catalyst surface (see schematic in Fig. 2b). Formation of this type of carbonate has been assigned to the direct adsorption of CO_2 within the surface oxygen vacancies by past studies [36,38]. Two more peaks were also observed at 1378 cm^{-1} and 1461 cm^{-1} on both catalysts, which were assigned to monodentate carbonate [37]. Therefore, it can be concluded that oxygen vacancy is one of the two sites for CO_2 adsorption. The adsorbed CO_2 at 400 °C on the Cu-Al spinel surface was then exposed to H_2 to observe the potential carbonate peak desorption. Surprisingly, no detectable carbonate desorption was observed after hydrogen introduction, which shows the strong interaction of CO_2 with the catalyst surface. We then conducted an *in-situ* DRIFTS experiment by co-feeding both CO_2 and H_2 while increasing the temperature to see the reaction on the Cu-Al spinel catalyst surface (Fig. 2c). At 350 °C, the gas phase CO was detected while the carbonate peaks were not much disturbed. Therefore, we concluded from the DRIFTS experiments that only a small proportion of the adsorbed CO_2 is reacting on the surface at this temperature to form the products while the rest is strongly bound to the surface. This is in agreement with the CO_2-TPD results which showed the strong adsorption of CO_2 on the catalyst surface. This is also in

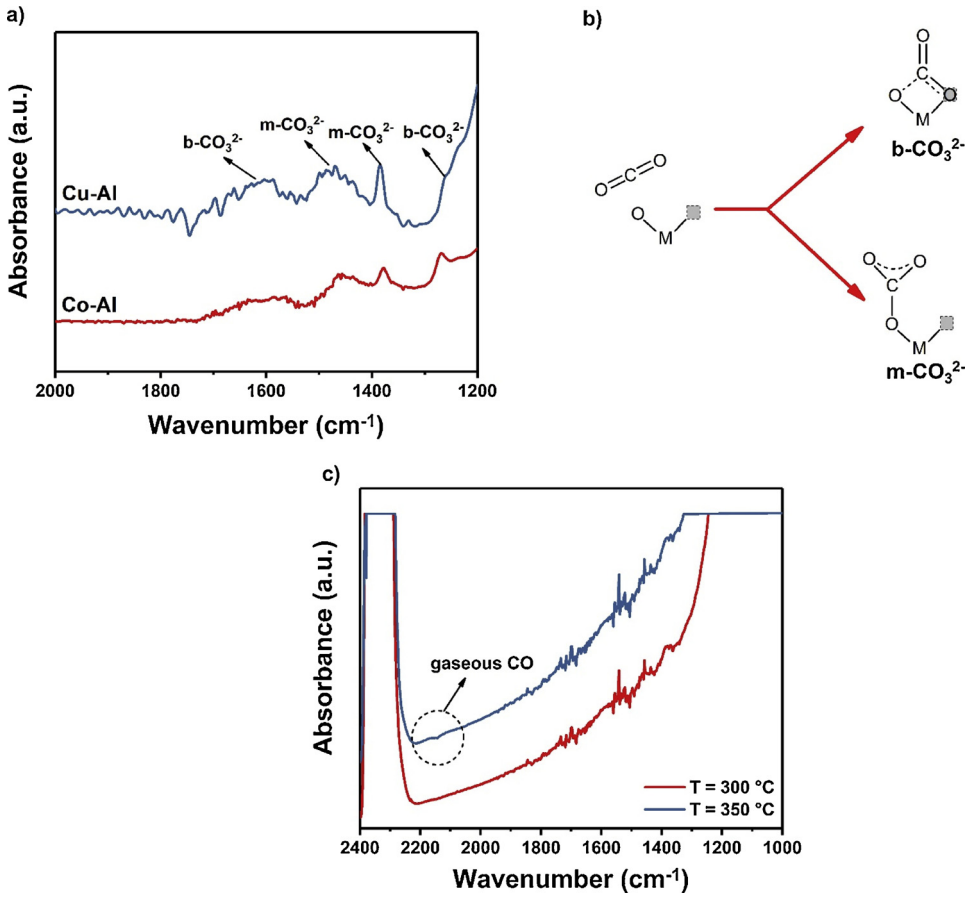

Fig. 2. a) DRIFT spectra acquired for CO_2 adsorption on the surface of Co-Al and Cu-Al spinel catalysts. b) Illustration of CO_2 adsorption on the catalysts surfaces. c) In-situ DRIFT spectra acquired through co-feeding of CO_2 and H_2 on the surface of Cu-Al spinel.

accordance with the low total conversion of CO_2 on this catalyst compared to the previous study [22]. None of the two identified carbonates were more active in the *in-situ* DRIFTS experiment. Therefore, we can conclude that the presence of oxygen vacancies on the surface of these two catalysts provides additional active sites for CO_2 adsorption, but the participation of monodentate carbonate in the reaction is not excluded. One way to observe CO_2 participation in the reaction, would be to use modulation excitation spectroscopy combined with phase sensitive detection which selectively enhances the signals of the species involved in the catalytic cycle and suppresses the signals of all static species as well as noise. More information about this technique can be found in the literature [39,40].

3.3. Oxygen vacancy formation

To better understand the structure-activity relationship of the Cu-Al and Co-Al spinel catalysts, XRD and XPS were used to investigate the atomic structure of these catalysts. Rietveld refinement showed only a slight degree of inversion in the Co-Al spinel structure, while for the Cu-Al spinel, this degree of inversion was much more pronounced. The occupancy of tetrahedral and octahedral sites is given for both catalysts in Table 1 (the Rietveld plots and structural parameters are presented in Figs. S2 and S3 and Table S3). A notably higher inversion degree, which was measured for the Cu-Al spinel, may have formed a more disordered structure, in which cations are partly substituted. Oxygen vacancies form in this structure to balance the positive charges and hence, more oxygen vacancies are formed in the structure with a more disordered spinel structure [41].

Because the catalytic reactions occur on the surface, the surface structure was independently investigated using XPS. The slight inversion degree of the Co-Al spinel appears absent on the catalyst surface. Deconvolution of the peaks observed for the Co 2p and Al 2p regions confirmed that Co atoms were only present in the tetrahedral positions and Al atoms only occupied the octahedral positions on the surface, forming a normal surface spinel (Fig. 3a) [42]. For the Cu-Al spinel, the deconvoluted peaks of the spectra corresponding to the Cu $2p_{3/2}$ and Cu $2p_{1/2}$ regions showed both tetrahedral and octahedral positions taken by Cu atoms (Fig. 3b) [43]. The Al 2p region also contained the Cu 3p peak. However, the Al atoms also occupied both tetrahedral and octahedral sites, which confirmed the disordered structure of the surface of this catalyst [41].

Table 1
The occupancy of tetrahedral and octahedral positions for Co-Al and Cu-Al spinel catalysts using XRD.

Co-Al	Occupancy (%)	Cu-Al	Occupancy (%)
Co (tetrahedral)	86	Cu (tetrahedral)	63(4)
Al (tetrahedral)	14	Al (tetrahedral)	37(4)
Co (octahedral)	7	Cu (octahedral)	19(2)
Al (octahedral)	93	Al (octahedral)	81(2)

According to several studies, the formation of a distorted inverse spinel can lead to the formation of more oxygen vacancies [41,44,45]. The O 1s spectra of both catalysts are deconvoluted into two main peaks (Fig. 3c). The first peak was assigned to the lattice oxygen (O_L) on the surface, while the second peak presents the surface adsorbed oxygen (O_A), which can form due to the adsorption of O_2 on an oxygen vacancy [46]. It may be noted that the O 1s spectra of both samples was slightly shifted towards higher binding energies which is why the lattice oxygen and the surface adsorbed oxygen peaks appeared at somewhat higher

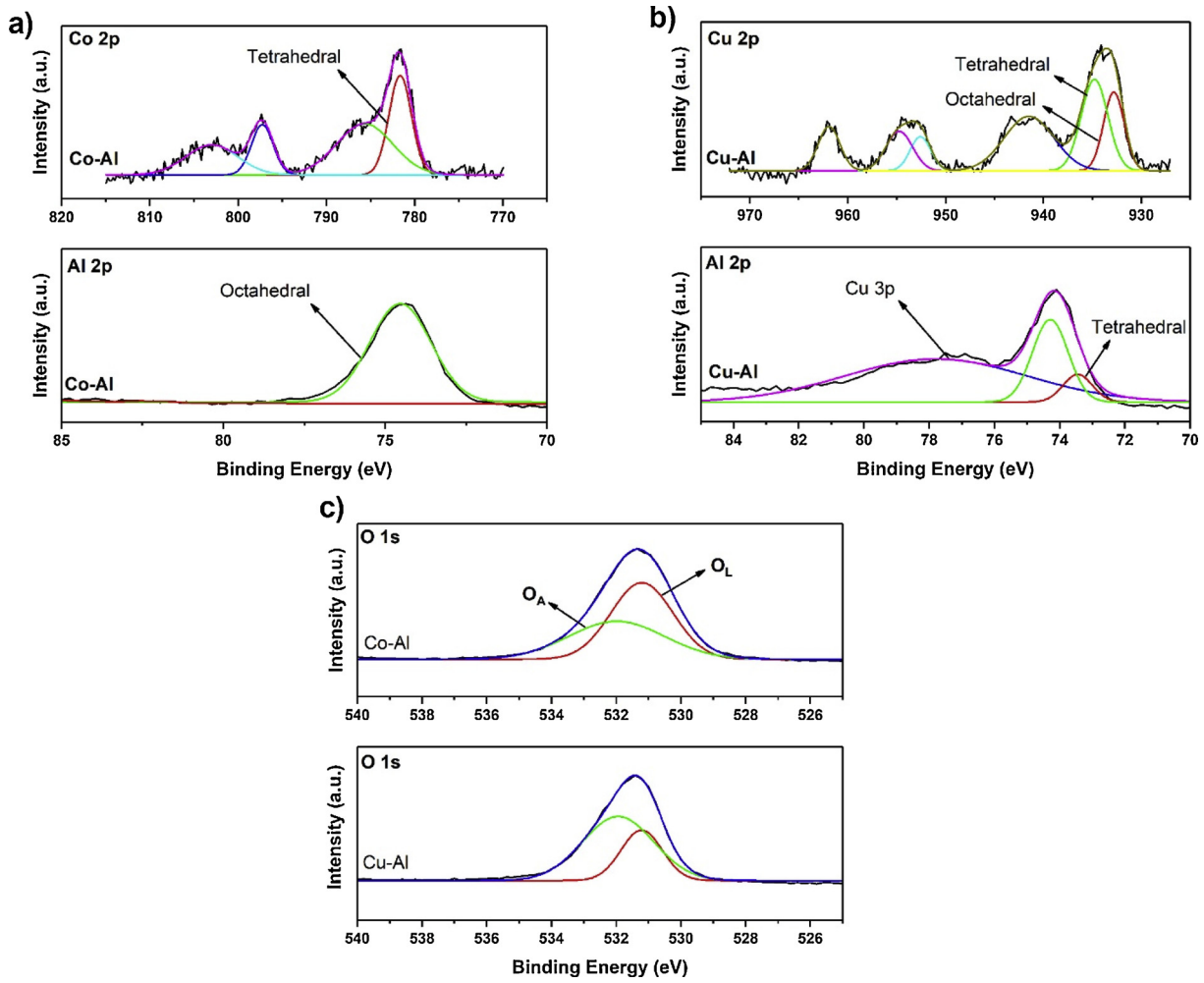

Fig. 3. a) Co 2p and Al 2p spectra for Co-Al spinel catalyst and b) Cu 2p and Al 2p spectra for Cu-Al spinel catalyst, and c) O 1s spectra for Co-Al and Cu-Al spinel catalysts.

binding energies. This, however, did not affect the results of our study. The $O_A/(O_A+O_L)$ ratio is higher for Cu-Al (0.68) compared to Co-Al (0.37). Therefore, a higher oxygen vacancy population was clearly formed on the Cu-Al spinel surface.

DFT was used as a tool to understand the difference in the energy of formation of oxygen vacancies on each surface based on the following equation:

$$E_{vac} = E_{M_{32}Al_{64}O_{127}} + \frac{1}{2}E_{O_2} - E_{M_{32}Al_{64}O_{128}} \quad \text{M= Cu, Co} \tag{1}$$

Where E_{vac} is the formation energy of an oxygen vacancy, $E_{M_{32}Al_{64}O_{127}}$ is the energy of the system containing an oxygen vacancy, $\frac{1}{2}E_{O_2}$ is half of the energy of an oxygen molecule, and $E_{M_{32}Al_{64}O_{128}}$ is the energy of the defect-free system. The modeled surfaces for both catalysts are presented in Fig. 4. In the case of the Cu-Al spinel, there are two types of oxygen atoms present on the surface, namely those that are three-coordinated (O_{3f}), which are coordinated with one copper and two aluminum atoms, and four-coordinated (O_{4f}), which are coordinated with one copper and three aluminum atoms. In the case of Co-Al spinel, there is only one type of surface oxygen atom, which is coordinated with three aluminum atoms on the surface.

The lowest formation energy of an oxygen vacancy was calculated to be 1.42 eV for the Cu-Al spinel system, which was based on subtraction of one O_{3f}. This calculated energy was found to be higher in the case of subtraction of a surface oxygen from Co-Al surface (1.84 eV) indicating that oxygen vacancies are more easily formed on the surface of the Cu-Al spinel catalyst. Therefore, the calculation agreed with the previously discussed results confirming that oxygen vacancy formation is more probable on the Cu-Al spinel surface.

In order to confirm the effect of oxygen vacancy density on the performance of the spinel catalysts in the RWGS reaction, we treated Co-Al with NaOH to create oxygen vacancies on the surface of this catalyst. In this method, Co-Al was treated with a 1 M aqueous solution of NaOH for 30 min (Co-Al-AT) and was washed thoroughly to avoid the presence of Na on the catalyst surface [31]. This catalyst was then tested at the same conditions for the RWGS reaction (Fig. 5a). The activity of the treated catalyst increased significantly compared to the Co-Al spinel. To confirm the formation of the oxygen vacancies, the O 1s spectra of the treated catalyst were collected using XPS and the O_A peak clearly increased due to the alkaline treatment (Fig. 5b).

This data is in agreement with the clear difference in the O 1s spectra for Co-Al and Cu-Al. The surface concentrations of Co and Al for both Co-Al spinel and Co-Al-AT spinel were measured to confirm that the alkaline treatment did not affect the metal concentrations. “T” and “NT” are used for treated and non-treated, respectively. Both ratios of Co_T/Co_{NT} and Al_T/Al_{NT} were found to be approximately 0.9, based on Co $2p_{3/2}$ and Al 2p peaks. Fig. 6 shows the relation between CO_2 conversion and $O_A/(O_A+O_L)$ ratio at the studied range of temperatures. An increase in activity can clearly be observed and even seems to follow a linear trend with respect to the $O_A/(O_A+O_L)$ ratio.

Therefore, this study shows that the high degree of inversion of the Cu-Al spinel structure compared to Co-Al system generated more oxygen vacancies on the catalyst surface, which, in turn, promoted the

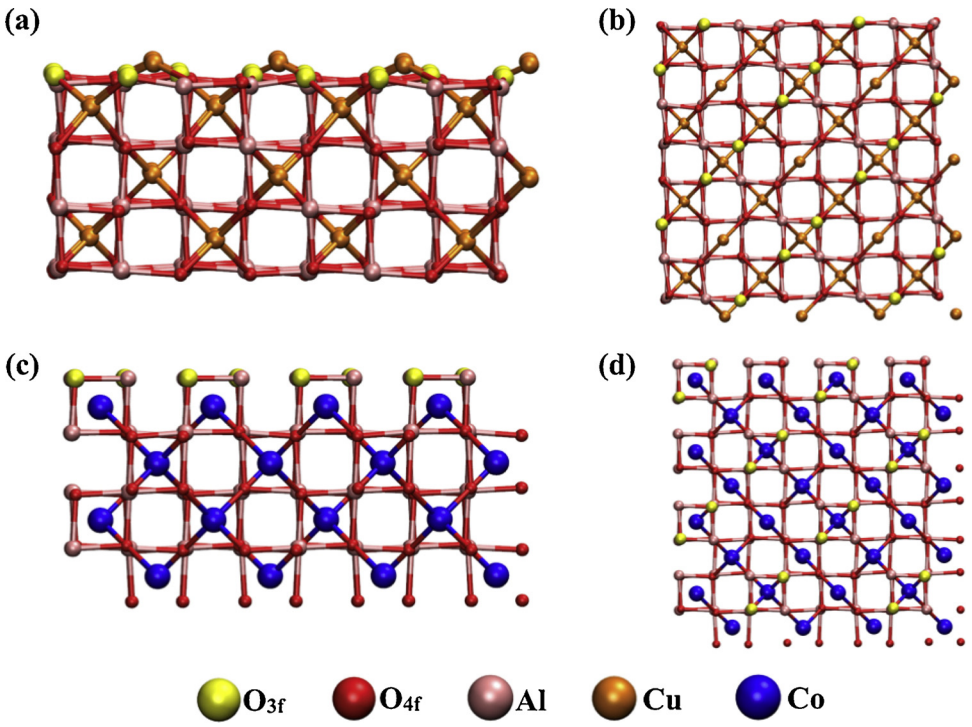

Fig. 4. Cu-Al and Co-Al spinel slabs with 224 atoms and similar box sizes. a) $CuAl_2O_4$ surface viewed from the y-direction and b) from the z-direction. c) $CoAl_2O_4$ surface viewed from the y-direction and d) from the z-direction. $CuAl_2O_4$ has threefold (O_{3f}) and fourfold (O_{4f}) coordinated oxygen atoms, whereas $CoAl_2O_4$ has only O_{3f} oxygen atoms on its surface.

adsorption and activation of CO_2 for the RWGS reaction. Based on this study, we found that the crystal structure (and its ability to form defects) played an important role in the catalytic activity of spinel oxides for the RWGS, even more important than the transition metals used for hydrogen adsorption/dissociation (such as Cu or Co). The ability of a structure to create oxygen vacancies should thus be considered when designing catalysts for this reaction.

4. Conclusion

Cu-Al spinel materials were previously proposed as active and stable catalysts for the catalytic hydrogenation of CO_2 to CO, also known as the Reverse Water Gas Shift (RWGS) reaction. In this study, the molecular basis of the activity of spinel oxides as catalysts for this reaction was investigated by comparing Cu-Al and Co-Al spinel oxides. Cu-Al outperformed Co-Al in the studied range of temperatures (250 °C–400 °C) despite its lower surface area and larger crystallite domain size. Further investigation of the catalyst with XRD and XPS showed that Cu-Al spinel formed a higher inversion degree, which caused the formation of a more disordered structure compared to Co-Al. Furthermore, a higher concentration of oxygen vacancies was present on the Cu-Al spinel surface. The idea of energetically favored formation of oxygen vacancies on the surface of Cu-Al spinel was further supported by calculation of the energy required to form oxygen vacancy on a spinel surfaces through a DFT study. DRIFT spectra as well as CO_2-TPD proposed that a large portion of the adsorbed CO_2 on the surface of both catalysts were located directly on the vacancies. Through DRIFTS experiment, it was also evident that only a small proportion of the adsorbed CO_2 molecules, i.e. weakly bound CO_2, were participating in the reaction in the studied temperature range, which was in agreement with the CO_2-TPD results as well as the catalytic tests. With regards to the Co-Al catalyst, higher activity was achieved once vacancies were deliberately formed on the surface through alkaline treatment of the catalyst. Therefore, oxygen vacancies appear to be critical to CO_2

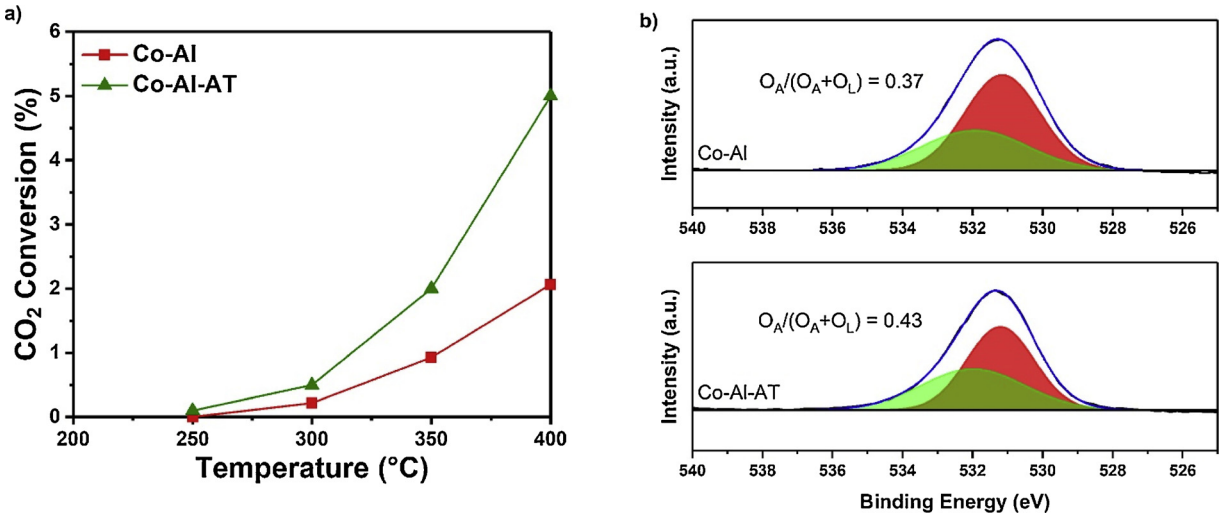

Fig. 5. a) Catalytic activity for Co-Al and Co-Al-AT spinel catalysts. b) O 1s spectra for Co-Al and Co-Al-AT spinel catalysts.

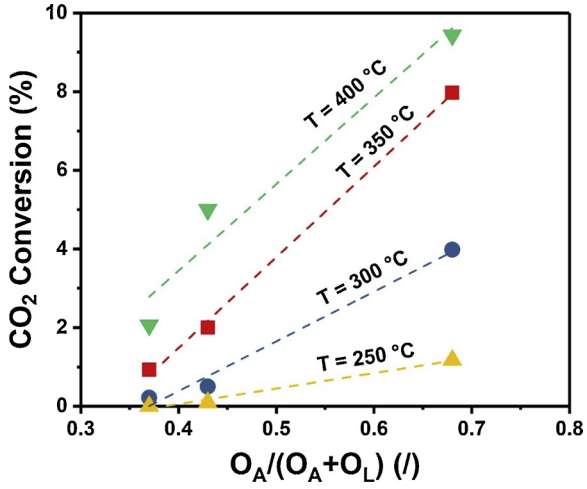

Fig. 6. Correlation between CO_2 conversion and the $O_A/(O_A+O_L)$ ratio. The presented values of the $O_A/(O_A+O_L)$ ratios are calculated for Co-Al (0.37), Co-Al-AT (0.43), and Cu-Al (0.68).

adsorption and activation on the spinel catalyst surfaces. For the specified temperature range, the spinel crystal structure was the key to adsorb and activate CO_2 for the RWGS reaction and, counterintuitively, the transition metals associated to the hydrogen adsorption/dissociation (Cu and Co) did not have a direct impact on the catalyst activity. The concentration of oxygen vacancies should be seen as a key variable to be controlled when designing spinel oxide catalysts for CO_2 activation.

Authors contributions

The manuscript was written through contributions of all authors. All authors have given approval to the final version of the manuscript. A.M.B, and O.K. planned the project. A.M.B. and F.H. conducted the experiments. P.S conducted the XRD experiments and provided input on the analysis. C.J.B. helped with the experiments procedure. M.K. and U.R. performed and supervised the computational part of this study, respectively. M.K. and U.R. wrote the computational studies section. J.S.L. and O.K. provided the facilities and helped with editing the manuscript. J.S.L. supervised the work done by F.H. O.K. supervised the project.

CRediT authorship contribution statement

Ali M. Bahmanpour: Conceptualization, Methodology, Investigation, Validation, Visualization, Writing - original draft. **Florent Héroguel:** Methodology, Validation, Visualization, Writing - original draft. **Murat Kılıç:** Software, Writing - original draft, Visualization. **Christophe J. Baranowski:** Investigation, Writing - original draft. **Pascal Schouwink:** Methodology, Investigation, Writing - original draft. **Ursula Röthlisberger:** Software, Supervision, Writing - review & editing, Funding acquisition. **Jeremy S. Luterbacher:** Supervision, Writing - review & editing, Funding acquisition. **Oliver Kröcher:** Supervision, Conceptualization, Funding acquisition, Writing - review & editing.

Declaration of Competing Interest

The authors declare that they have no known competing financial interests or personal relationships that could have appeared to influence the work reported in this paper.

Acknowledgments

The authors are grateful for the funding provided by EPFL. This research project is part of the Swiss Competence Center for Energy Research SCCER BIOSWEET of the Swiss Innovation Agency Innosuisse. Florent Héroguel and Jeremy S. Luterbacher acknowledge funding from the Swiss National Science Foundation through grant PYAPP2_154281. The authors would like to acknowledge Pierre Mettraux for XPS analysis, and Sylvain Coudret for ICP-OES analysis. M. Kılıç and U. Röthlisberger acknowledge HPC resources of CSCS (Swiss National Supercomputer Centre).

Appendix A. Supplementary data

Supplementary material related to this article can be found, in the online version, at doi:https://doi.org/10.1016/j.apcatb.2020.118669.

References

[1] J.C. Zachos, G.R. Dickens, R.E. Zeebe, An early Cenozoic perspective on greenhouse warming and carbon-cycle dynamics, Nature 451 (2008) 279–283.
[2] F. Arena, K. Barbera, G. Italiano, G. Bonura, L. Spadaro, F. Frusteri, Synthesis, characterization and activity pattern of Cu-ZnO/ZrO_2 catalysts in the hydrogenation of carbon dioxide to methanol, J. Catal. 249 (2007) 185–194.
[3] M.D. Porosoff, B. Yan, J.G. Chen, Catalytic reduction of CO_2 by H_2 for synthesis of CO, methanol and hydrocarbons: challenges and opportunities, Energy Environ. Sci. 9 (2016) 62–73.
[4] R.G. Herman, K. Klier, G.W. Simmons, B.P. Finn, J.B. Bulko, T.P. Kobylinski, Catalytic synthesis of methanol from CO H_2. I. Phase composition, electronic properties, and activities of the Cu/ZnO/M_2O_3 catalysts, J. Catal. 56 (1979) 407–429.
[5] G.C. Chinchen, P.J. Denny, J.R. Jennings, M.S. Spencer, K.C. Waugh, Synthesis of methanol. Part 1. Catalysts and kinetics, Appl. Catal. 36 (1988) 1–65.
[6] J.H. Kwak, L. Kovarik, J. Szanyi, Heterogeneous catalysis on atomically dispersed supported metals: CO_2 reduction on multifunctional Pd catalysts, ACS Catal. 3 (2013) 2094–2100.
[7] I.A. Fisher, A.T. Bell, A comparative study of CO and CO_2 hydrogenation over Rh/SiO_2, J. Catal. 162 (1996) 54–65.
[8] W. Wang, S. Wang, X. Ma, J. Gong, Recent advances in catalytic hydrogenation of carbon dioxide, Chem. Soc. Rev. 40 (2011) 3703–3727.
[9] C. Álvarez Galván, J. Schumann, M. Behrens, J.L.G. Fierro, R. Schlögl, E. Frei, Reverse water-gas shift reaction at the Cu/ZnO interface: influence of the Cu/Zn ratio on structure-activity correlations, Appl. Catal. B Environ. 195 (2016) 104–111.
[10] C.S. Chen, J.H. Lin, J.H. You, C.R. Chen, Properties of Cu(thd)2 as a precursor to prepare Cu/SiO_2 catalyst using the atomic layer epitaxy technique, J. Am. Chem. Soc. 128 (2006) 15950–15951.
[11] C.-S. Chen, W.-H. Cheng, S.-S. Lin, Study of iron-promoted Cu/SiO_2 catalyst on high temperature reverse water gas shift reaction, Appl. Catal. Gen. 257 (2004) 97–106.
[12] C.-S. Chen, W.-H. Cheng, S.-S. Lin, Study of reverse water gas shift reaction by TPD, TPR and CO_2 hydrogenation over potassium-promoted Cu/SiO_2 catalyst, Appl. Catal. Gen. 238 (2002) 55–67.
[13] X. Yang, X. Su, X. Chen, H. Duan, B. Liang, Q. Liu, X. Liu, Y. Ren, Y. Huang, T. Zhang, Promotion effects of potassium on the activity and selectivity of Pt/zeolite catalysts for reverse water gas shift reaction, Appl. Catal. B Environ. 216 (2017) 95–105.
[14] C.-S. Chen, W.-H. Cheng, S.-S. Lin, Mechanism of CO formation in reverse water-gas shift reaction over Cu/Al_2O_3 catalyst, Catal. Lett. 68 (2000) 45–48.
[15] L. Lin, S. Yao, Z. Liu, F. Zhang, N. Li, D. Vovchok, A. Martínez-Arias, R. Castaneda, J. Lin, S.D. Senanayake, D. Su, D. Ma, J.A. Rodriguez, In situ characterization of Cu/CeO_2 nanocatalysts for CO_2 hydrogenation: morphological effects of nanostructured ceria on the catalytic activity, J. Phys. Chem. C 122 (2018) 12934–12943.
[16] X. Zhang, X. Zhu, L. Lin, S. Yao, M. Zhang, X. Liu, X. Wang, Y.-W. Li, C. Shi, D. Ma, Highly dispersed copper over β-Mo_2C as an efficient and stable catalyst for the reverse water gas shift (RWGS) reaction, ACS Catal. 7 (2017) 912–918.
[17] N. Nityashree, C.A.H. Price, L. Pastor-Perez, G.V. Manohara, S. Garcia, M.M. Maroto-Valer, T.R. Reina, Carbon stabilised saponite supported transition metal-alloy catalysts for chemical CO_2 utilisation via reverse water-gas shift reaction, Appl. Catal. B Environ. 261 (2020).
[18] Q. Zhang, L. Pastor-Pérez, W. Jin, S. Gu, T.R. Reina, Understanding the promoter effect of Cu and Cs over highly effective B-Mo_2C catalysts for the reverse water-gas shift reaction, Appl. Catal. B Environ. 244 (2019) 889–898.
[19] C. Liu, S.L. Nauert, M.A. Alsina, D. Wang, A. Grant, K. He, E. Weitz, M. Nolan, K.A. Gray, J.M. Notestein, Role of surface reconstruction on Cu/TiO_2 nanotubes for CO_2 conversion, Appl. Catal. B Environ. 255 (2019).
[20] S. Yao, X. Zhang, W. Zhou, R. Gao, W. Xu, Y. Ye, L. Lin, X. Wen, P. Liu, B. Chen, E. Crumlin, J. Guo, Z. Zuo, W. Li, J. Xie, L. Lu, C.J. Kiely, L. Gu, C. Shi, J.A. Rodriguez, D. Ma, Atomic-layered Au clusters on α-MoC as catalysts for the low-temperature water-gas shift reaction, Science. 357 (2017).
[21] M. Xu, S. Yao, D. Rao, Y. Niu, N. Liu, M. Peng, P. Zhai, Y. Man, L. Zheng, B. Wang,

B. Zhang, D. Ma, M. Wei, Insights into interfacial synergistic catalysis over Ni@TiO_{2-x} catalyst toward water-gas shift reaction, J. Am. Chem. Soc. 140 (2018) 11241–11251.
[22] A.M. Bahmanpour, F. Héroguel, M. Kılıç, C.J. Baranowski, L. Artiglia, U. Röthlisberger, J.S. Luterbacher, O. Kröcher, Cu–Al spinel as a highly active and stable catalyst for the reverse water gas shift reaction, ACS Catal. 9 (2019) 6243–6251.
[23] M.S. Jeletic, M.T. Mock, A.M. Appel, J.C. Linehan, A cobalt-based catalyst for the hydrogenation of CO_2 under ambient conditions, J. Am. Chem. Soc. 135 (2013) 11533–11536.
[24] Y. Zhang, G. Jacobs, D.E. Sparks, M.E. Dry, B.H. Davis, CO and CO_2 hydrogenation study on supported cobalt Fischer-Tropsch synthesis catalysts, Catal. Today 71 (2002) 411–418.
[25] M.D. Porosoff, X. Yang, J.A. Boscoboinik, J.G. Chen, Molybdenum carbide as alternative catalysts to precious metals for highly selective reduction of CO_2 to CO, Angew. Chem. Int. Ed. 53 (2014) 6705–6709.
[26] J.E. Baker, R. Burch, N. Yuqin, Investigation of $CoAl_2O_4$, Cu/$CoAl_2O_4$ and Co/$CoAl_2O_4$ catalysts for the formation of oxygenates from a carbon monoxide-carbon dioxide-hydrogen mixture, Appl. Catal. 73 (1991) 135–152.
[27] H. Muneam, S. Hadi, M.M. Kareem, S.D. Jackson, Preparation and characterization of (Co,Mn)(Co,Mn)$_2O_4$/MgO catalysts, Int. J. Ind. Chem. 7 (2016) 93–101.
[28] G. Li, C. Gu, W. Zhu, X. Wang, X. Yuan, Z. Cui, H. Wang, Z. Gao, Hydrogen production from methanol decomposition using Cu-Al spinel catalysts, J. Clean. Prod. 183 (2018) 415–423.
[29] A. Alejandre, F. Medina, P. Salagre, A. Fabregat, J.E. Sueiras, Characterization and activity of copper and nickel catalysts for the oxidation of phenol aqueous solutions, Appl. Catal. B Environ. 18 (1998) 307–315.
[30] S. Sato, M. Iijima, T. Nakayama, T. Sodesawa, F. Nozaki, Vapor-phase dehydrocoupling of methanol to methyl formate over $CuAl_2O_4$, J. Catal. 169 (1997) 447–454.
[31] Y. Liu, B. Wei, L. Xu, H. Gao, M. Zhang, Generation of oxygen vacancy and OH radicals: a comparative study of Bi_2WO_6 and Bi_2WO_{6-x} nanoplates, ChemCatChem 7 (2015) 4076–4084.
[32] A.A. Coelho, Whole-profile structure solution from powder diffraction data using simulated annealing, J. Appl. Crystallogr. 33 (2000) 899–908.
[33] P. Giannozzi, S. Baroni, N. Bonini, M. Calandra, R. Car, C. Cavazzoni, D. Ceresoli, G.L. Chiarotti, M. Cococcioni, I. Dabo, A. Dal Corso, S. De Gironcoli, S. Fabris, G. Fratesi, R. Gebauer, U. Gerstmann, C. Gougoussis, A. Kokalj, M. Lazzeri, L. Martin-Samos, N. Marzari, F. Mauri, R. Mazzarello, S. Paolini, A. Pasquarello, L. Paulatto, C. Sbraccia, S. Scandolo, G. Sclauzero, A.P. Seitsonen, A. Smogunov, P. Umari, R.M. Wentzcovitch, QUANTUM ESPRESSO: a modular and open-source software project for quantum simulations of materials, J. Phys. Condens. Matter 21 (2009).
[34] J.P. Perdew, K. Burke, Generalized gradient approximation for the exchange-correlation hole of a many-electron system, Phys. Rev. B - Condens. Matter Mater. Phys. 54 (1996) 16533–16539.
[35] H.J. Monkhorst, J.D. Pack, Special points for Brillouin-zone integrations, Phys. Rev. B 13 (1976) 5188–5192.
[36] X. Liu, M. Wang, C. Zhou, W. Zhou, K. Cheng, J. Kang, Q. Zhang, W. Deng, Y. Wang, Selective transformation of carbon dioxide into lower olefins with a bifunctional catalyst composed of $ZnGa_2O_4$ and SAPO-34, Chem. Commun. 54 (2017) 140–143.
[37] A.M. Turek, I.E. Wachs, E. DeCanio, Acidic properties of alumina-supported metal oxide catalysts: an infrared spectroscopy study, J. Phys. Chem. 96 (1992) 5000–5007.
[38] B. Liu, C. Li, G. Zhang, X. Yao, S.S.C. Chuang, Z. Li, Oxygen vacancy promoting dimethyl carbonate synthesis from CO_2 and methanol over Zr-doped CeO_2 nanorods, ACS Catal. 8 (2018) 10446–10456.
[39] A. Urakawa, T. Bürgi, A. Baiker, Sensitivity enhancement and dynamic behavior analysis by modulation excitation spectroscopy: principle and application in heterogeneous catalysis, Chem. Eng. Sci. 63 (2008) 4902–4909.
[40] D. Ferri, M.A. Newton, M. Nachtegaal, Modulation excitation X-ray absorption spectroscopy to probe surface species on heterogeneous catalysts, Top. Catal. 54 (2011) 1070–1078.
[41] H. Nguyen-Phu, E.W. Shin, Disordered structure of $ZnAl_2O_4$ phase and the formation of a Zn NCO complex in ZnAl mixed oxide catalysts for glycerol carbonylation with urea, J. Catal. 373 (2019) 147–160.
[42] X. Duan, D. Yuan, F. Yu, Cation distribution in Co-doped $ZnAl_2O_4$ nanoparticles studied by X-ray photoelectron spectroscopy and 27Al solid-state NMR spectroscopy, Inorg. Chem. 50 (2011) 5460–5467.
[43] F. Severino, J.L. Brito, J. Laine, J.L.G. Fierro, A. López Agudo, Nature of copper active sites in the carbon monoxide oxidation on $CuAl_2O_4$ and $CuCr_2O_4$ spinel type catalysts, J. Catal. 177 (1998) 82–95.
[44] G.K. Behrh, M. Isobe, F. Massuyeau, H. Serier-Brault, E.E. Gordon, H.-J. Koo, M.-H. Whangbo, R. Gautier, S. Jobic, Oxygen-vacancy-induced midgap states responsible for the fluorescence and the long-lasting phosphorescence of the inverse spinel Mg(Mg,Sn)O_4, Chem. Mater. 29 (2017) 1069–1075.
[45] J.M. Costa, L.C. Lima, M.S. Li, I.M.G. Santos, M.R.S. Silva, A.S. Maia, Structural and photocatalytic properties of Mg_2SnO_4 spinel obtained by modified Pechini method, Mater. Lett. 236 (2019) 320–323.
[46] X. Wang, Z. Lan, K. Zhang, J. Chen, L. Jiang, R. Wang, Structure-activity relationships of AMn_2O_4(A = Cu and Co) spinels in selective catalytic reduction of NO_x: experimental and theoretical study, J. Phys. Chem. C 121 (2017) 3339–3349.